MATERIALS CHEMISTRY FRONTIERS

RESEARCH ARTICLE

View Article Online
View Journal | View Issue

Cite this: *Mater. Chem. Front.*, 2022, **6**, 3225

An efficient solution-processable non-doped hybridized local and charge-transfer (HLCT) emitter for a simplified organic light-emitting diode†

Thidarat Loythaworn,[a] Sujinda Petdee,[a] Pongsakorn Chasing,[a] Nuttapong Chantanop,[a] Pattarawadee Therdkatanyuphong,[a] Wijitra Waengdongbung,[b] Taweesak Sudyoadsuk[a] and Vinich Promarak *[ab]

Received 5th May 2022,
Accepted 6th September 2022

DOI: 10.1039/d2qm00401a

rsc.li/frontiers-materials

Here, a new solution-processable hybridized local and charge-transfer (HLCT) fluorescent molecule, **CPBzFC**, is designed and synthesized as an efficient emitter for low-cost and simple-structured electroluminescent devices. **CPBzFC** contains 7-(4-(carbazol-*N*-yl)phenyl)benzothiadiazole as an HLCT fragment directly linked to a hole-transporting and highly soluble 7-(3,6-di-*tert*-butylcarbazol-*N*-yl)-9,9′-bis(8-(3,6-di-*tert*-butylcarbazol-*N*-yl)octyl)fluorene part. The photophysical results and theoretical calculations unveil an HLCT excited-state character with a strong yellowish-green fluorescence emission (a solid-state photoluminescence quantum yield of 82%), decent hole-transporting mobility, good film morphology, and thermal and electrochemical stabilities. **CPBzFC** is successfully utilized as a solution-processed non-doped emitter in simple structured OLEDs. This device achieves excellent electroluminescence (EL) performance with an ultra-high brightness of 30 800 cd m^{-2}, a maximum external quantum efficiency (EQE_{max})of 6.74%, a maximum current efficiency (CE_{max}) of 14.38 cd A^{-1}, and a high exciton utilization efficiency (EUE) of 41%.

Introduction

Since a pioneering work on organic light-emitting diodes (OLEDs) reported by Tang and Vanslyke in 1987,[1] research in this field has been flourishing.[2–5] Over the past few years, the electroluminescence (EL) performance of OLEDs has steadily improved, making them a promising alternative to many of today's display and lighting technologies.[6] To date, OLED technology has become popular across various end-use industries and is quickly taking over the conventional display technologies (LCDs and LEDs). This is due to the fact that OLEDs provide the best image quality, are more efficient, are simpler to make, consume less power, are flexible, and reliable than other types of displays. One of the keys to this advancement is the development of high-performance light-emitting materials,[7,8] particularly, the recent advance in organic emitters that can theoretically realize a 100% internal quantum efficiency (IQE) by converting non-radiative triplet (T) excitons into radiative singlet (S) excitons *via* a reverse intersystem crossing (RISC) process of either the lowest triplet state (T_1) or high-lying triplet states (T_n; $n > 1$) known as thermally activated delayed fluorescence (TADF)[9–12] and hybridized local and charge-transfer (HLCT), respectively.[13–17] Between the two, the HLCT mechanism involves a conversion of a much short exciton lifetime of high-lying triplet states, which occurs on a nanosecond time scale, benefiting not only 100% IQE in a short time but also enabling lessen of a triplet accumulation process and thus improving the efficiency roll-off of the OLEDs. Therefore, HLCT fluorophores as non-doped emitters could be a promising candidate for practical uses. So far, several highly efficient HLCT molecules have been developed as emitters for OLEDs, including phenanthroimidazole derivatives as blue to deep-blue HLCT fluorophores,[18–24] triarylamine-benzothiadiazoles (Bz) as green to red-orange HCLT fluorophores,[15,25–29] and triarylamine-naphthothiadiazoles (NZ)[15,30–35] as red to near-infrared (NIR) HLCT fluorophores. However, all of them were fabricated by thermal vacuum deposition, involving heating a solid material inside a high vacuum chamber at high temperatures and in a small area which is not applicable for fabricating flexible and large area-size devices and scaling up for commercial applications. To this point, there are only a few examples of solution-processed HLCT-based OLED devices (Table S1, ESI†),[36–39] and their EL

[a] *Department of Materials Science and Engineering, School of Molecular Science and Engineering, Vidyasirimedhi Institute of Science and Technology, Wangchan, Rayong 21210, Thailand. E-mail: vinich.p@vistec.ac.th*
[b] *Research Network of NANOTEC-VISTEC on Nanotechnology for Energy, Vidyasirimedhi Institute of Science and Technology, Wangchan, Rayong 21210, Thailand*

† Electronic supplementary information (ESI) available. See DOI: https://doi.org/10.1039/d2qm00401a

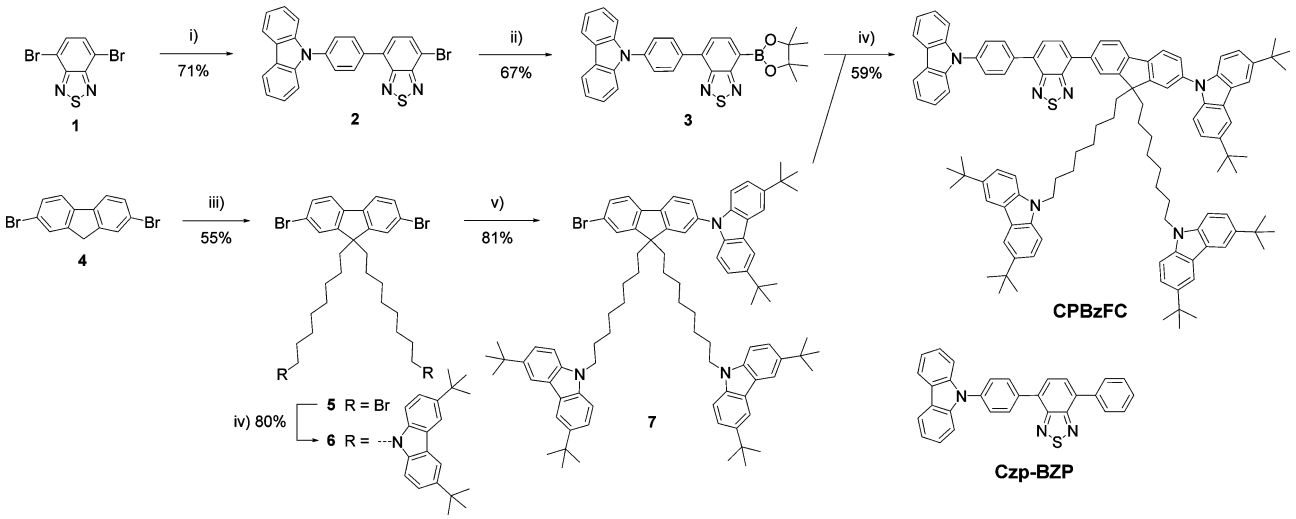

Scheme 1 Synthesis of **CPBzFC**. Reagents and conditions: (i) (4-(carbazol-*N*-yl)phenyl)boronic acid, $Pd(PPh_3)_4$, 10% K_2CO_3 (aq), THF, reflux; (ii) bispinacolatodiboron, KOAc, $Pd(dppf)_2Cl_2$, toluene, reflux; (iii) 1,8-dibromooctane, *tert*-$BuNH_4Br$, KOH, DFM, H_2O; (iv) 3,6-di-*tert*-butylcarbazole, KOH, DMF; (v) 3,6-di-*tert*-butylcarbazole, CuI, K_3PO_4, (±)-*trans*-1,2-diaminocyclohexane, toluene, reflux; (vi) $Pd(PPh_3)_4$, 10% K_2CO_3 (aq), THF, reflux.

performances are still inferior compared to their related thermal evaporated ones.[38,40] Hence, this work presents the design, synthesis, and properties of a high solid-state fluorescent molecule, namely CPBzFC (Scheme 1), bearing a combination of an HLCT feature and solution processability as an efficient non-doped emitter for a simple solution-processed OLED.[41] In this design, (4-(carbazol-*N*-yl)phenyl)benzothiadiazoles (CBzs) as a donor–acceptor (D–A) HLCT part are directly attached to the 7-(3,6-di-*tert*-butylcarbazol-*N*-yl)-9,9′-bis(8-(3,6-di-*tert*-butylcarbazol-*N*-yl)-octyl)fluorene moiety as an aromatic substituent. As a reference, a twisting D–A molecule 4-(4-(carbazol-9-yl)phenyl)-7-phenylbenzothiadiazole (CzP-BZP) (Scheme 1)[25] showed a special excited state character of the combined HLCT state and ''hot exciton'' features, which have been examined by the solvatochromic experiment and quantum chemical calculations. Interestingly, it surely harvested an EUE up to 48% in nondoped fluorescent OLEDs, breaking through 25% upper limit of spin-statistics. The 7-(3,6-di-*tert*-butylcarbazol-*N*-yl)-9,9′-bis(8-(3,6-di-*tert*-butylcarbazol-*N*-yl)octyl)fluorene will offer a combined properties of good organic solvent solubility and hole-transporting ability from its pendant 3,6-di-*tert*-butyl-8-octylcarbazoles.[42–44] Indeed, CPBzFC emits an intense yellowish-green color with HLCT properties, and thus, its simple solution-processed non-doped OLED accomplishes an outstanding EL performance (EQE = 6.74%) and a high EUE of 41%, which is comparable to the EL performance of its paternal HLCT molecule CzP-BZP-based thermal evaporated multiple layered OLED (EQE_{max} = 6.95%, EUE = 48%).[25]

Results and discussion

Scheme 1 outlines the synthesis of the designed HLCT emitter **CPBzFC**. Firstly, pinacol boronate ester **3** was prepared by a site-selective cross-coupling reaction of 4,7-dibromobenzo thiadiazole **1** with (4-(carbazol-*N*-yl)phenyl)boronic acid followed by a borylation of the resultant **2** with bis(pinacolato)diboron catalyzed with $Pd(dppf)_2Cl_2$/KOAc. Secondly, fluorenyl bromide **7** was synthesized by the alkylation of dibromofluorene **4** with an excess of 1,8-dibromooctane in the presence of KOH to yield dialkylated fluorene **5**. The nucleophilic substitution of **5** with 3,6-di-*tert*-butylcarbazole catalyzed by KOH followed by an Ullmann coupling reaction of the resultant **6** with 3,6-di-*tert*-butylcarbazole using (±)-*trans*-1,2-diaminocyclohexane/CuI/K_3PO_4 as a catalytic system. Finally, the Suzuki cross-coupling reaction of intermediates **3** and **7** catalyzed by $Pd(PPh_3)_4/K_2CO_3$ afforded **CPBzFC** as yellow solids in 59% yield. All synthesized compounds were unambiguously characterized by standard methods (^{1}H-NMR, ^{13}C-NMR, and high-resolution MS), and the results agreed with their chemical structures. **CPBzFC** exhibited good solubility in most organic solvents owning to its bulky molecular geometry and the presence of bis(8-(3,6-di-*tert*-butylcarbazol-*N*-yl)octyl)fluorene as a solubilizing moiety,[41] which allows the good quality thin film to be prepared by simple solution-processed casting techniques.

The photophysical properties of **CPBzFC** were analyzed in both the dilute solution and neat film, as shown in Fig. 1, and the data are presented in Table 1. The UV-vis absorption spectrum in toluene exhibited three distinct absorption bands at 298 nm attributed to the characteristic π–π* transition of the electron-rich carbazole,[45] 321 nm assigned to π–π* electronic transitions of the aromatic conjugated backbone, and 419 nm ascribed to the intramolecular charge transfer (ICT) transition from the electron-donating (D) carbazole to the electron-accepting (A) Bz unit of the HLCT part in the molecule. In the solution, CPBzFC showed an intense green fluorescence with an emission peak at 569 nm (Fig. 1) and a unit absolute fluorescence quantum yield (Φ_{PL} = 100%), indicating a very effective radiative electronic transition on the molecular backbone with negligible non-radiative losses. In the thin film, the

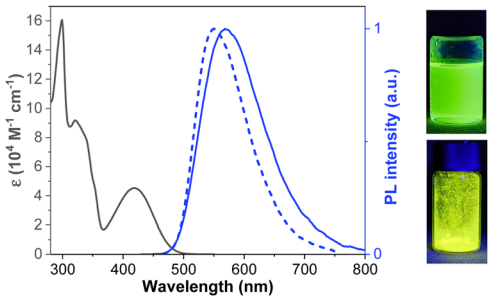

Fig. 1 UV-vis absorption and PL spectra (excited at 410 nm) in toluene solution (1.04×10^{-5} M) (solid line) and neat films coated on fused silica substrates (dashed line) (inset: photographs of emissions of solution and powder under irradiation with a 365 nm UV lamp).

molecule kept a strong emission peaked at 550 nm with its Φ_{PL} value marginally decreasing to 82%, signaling a certain degree of intermolecular interactions existing in the film state.

The absorption and PL behaviors of **CPBzFC** in different solvents were further examined to study the solvatochromic effect. As depicted in Fig. 2a, the absorption spectra display virtually unchanged profiles (shape and position) with changing solvent polarity, indicating that the ground-state dipole moment of the molecule is slightly disturbed by solvent variation. Conversely, the PL spectra tend to shift to the long-wavelength (from 527 nm in triethylamine (TEA) to 560 nm in tetrahydrofuran (THF) and 636 nm in dimethylformamide (DMF)) with an increasing broadening of the emission band as the solvent polarity increases, suggesting that the excited-state dipole moment of the molecule is highly dependent on the solvent polarity or the singlet higher excited state is more polar than the lower ground state.[46,47] So the emission spectra are more affected by the polarity of the solvent than the absorption spectra, which suggests that a large CT taking place in the excited state.[48] Additionally, the Φ_{PL} values of **CPBzFC** in different solvents exhibited a decreasing trend from 100% in toluene to 65% in dichloromethane, and 5% in acetonitrile. The fluorescence efficiency of molecular systems that endure effective ICT upon photoexcitation decreases down to competing excited electron transfer from the donor to the acceptor site resulting in quenching of fluorescence.[49–51] This solvatochromic behavior proves the existence of a charge CT character in the excited state of **CPBzFC**.

To inspect the effect of solvents on the emission properties of the molecule, the correlation between the Stokes shift

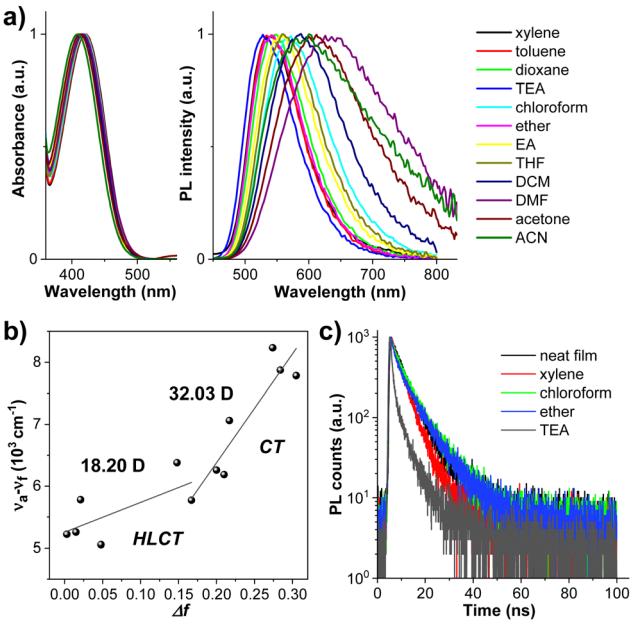

Fig. 2 (a) Normalized UV-vis absorption and PL spectra in different solvents. (b) Linear fitting of the Lippert–Mataga model between the Stokes shift ($\nu_a - \nu_f$) and the solvent polarity function (Δf). (c) Transient PL decay spectra in low polarity solvents and neat films.

($\nu_a - \nu_f$) and the solvent polarity function (Δf) was plotted following the Lippert–Mataga equation,[52] which describes the interactions between the solvent and dipole moment of the fluorophore. As shown in Fig. 2b, the plot displays two linear sections in low-polarity and high-polarity regions, defining the existence of two different excited states.[53] As a result, the excited-state dipole moments (μ_e) can be estimated to be 18.20 D in low-polarity solvents ($\Delta f \leq 0.15$) and 32.03 D in high-polarity solvents ($\Delta f \geq 0.15$). The small μ_e value of 18.20 D is slightly higher than that of the common LE fluorophores,[54] and close to that of a typical HLCT molecule *N*,*N*-diphenyl-4-(9-phenylnaphthothiadiazol-4-yl)aniline (TPA-NZP) (μ_e = 17.50 D),[15] denoting that in low-polarity solvents the emissive S_1 state of **CPBzFC** retained a small part of the CT components in addition to LE.[55] Besides, the large μ_e value of 32.03 D is slightly more than that of a standard CT molecule 4-(*N*,*N*-dimethylamino)benzonitrile (DMABN) (μ_e = 23 D),[56] ascribing to the usual CT-like excited-state. Thus, **CPBzFC** was a typical D–A dipolar molecule with a CT-dominated state in more and medium polar solvents and a mixed contribution of LE and CT states in less

Table 1 Key physical data of the synthesized **CPBzFC** fluorophore

$\lambda_{abs}(\varepsilon)^a$ (nm, 10^4 M^{-1} cm^{-1})	λ_{PL} (nm) sol[a]/film[b]	τ^c (ns) sol[a]/film[b]	$\Phi_{PL}{}^d$ (%) sol[a]/film[b]	$T_g/T_{5d}{}^e$ (°C)	$E_{1/2}$ *vs.* Ag/Ag^{+} [f] (V)	E_g^{opt}/E_g^{ele} [g] (eV)	HOMO/LUMO[h] (eV)	Hole mobility[i] (cm^2 V^{-1} s^{-1})
298 (16.09), 321 (9.17), 419 (4.55)	569/550	6.35/5.85	100/82	147/421	−1.39, 1.15, 1.38	2.53/2.41	−5.51/−2.98	7.54×10^{-7}

[a] Measured in dilute toluene. [b] Measured in thin films coated on fused silica substrates. [c] Transient PL decay lifetime. [d] Absolute PL quantum yield measured using an integrating sphere. [e] Measured by DSC (2nd scan) and TGA under a N_2 flow. [f] Obtained from the CV measurement at 50 mV s^{-1}. [g] Estimated from the onset of the absorption spectra in thin films: $E_g^{opt} = 1240/\lambda_{onset}$ and $E_g^{ele} = E_{onset}^{ox} - E_{onset}^{re}$, where E_{onset}^{ox} and E_{onset}^{re} are the onset potential of the oxidation and reduction, respectively. [h] Calculated from the onset redox potential of cyclic voltammetry: HOMO (eV) = $-(4.44 + E_{onset}^{ox})$ and LUMO (eV) = HOMO + E_g^{opt}. [i] Obtained from HOD (ITO/PEDOT : PSS/CPBzFC/MoO_3/Al).

polar solvents. In addition, the Φ_{PL} value of **CPBzFC** decreases with the increasing solvent polarity, and a relatively high Φ_{PL} was obtained in low polarity media (xylene (100%), chloroform (100%), ether (100%), TEA (100%), and neat film (82%)), signifying that a certain degree of the LE character has been introduced; therefore, the emissive S_1 state in low polar solvents comprised both CT and LE components. The interstate coupling of LE with CT creates a new HLCT emissive state. The HLCT state of **CPBzFC** in low polarity media ($\Delta f \geq 0.15$) (xylene, chloroform, ether, TEA, and neat films) was confirmed by transient PL decay measurements (Fig. 2c). The spectra displayed single-exponential decay profiles and short lifetimes (2.70 ns for TEA, 4.80 ns for xylene, 5.6 1 ns for ether, 5.85 ns for neat films, and 6.35 ns for chloroform), verifying that the excited state responsible for the PL emission of this D–A architecture initiates from one hybridized LE and CT excited state, forming an HLCT state rather than a simple mix-up of two LE and CT states.[57,58] This finding is also in compliance well with the results of the theoretical calculation, as discussed below (Fig. 3).

To study the electronic properties of **CPBzFC**, density functional theory (DFT) calculations were carried out with the ground-state structure optimized to a minimum using the B3LYP/6-31G(d,p) level of theory. As depicted in Fig. 3a, its lowest unoccupied molecular orbital (LUMO) is mainly localized on the Bz ring with a small contribution from the adjacent phenyl rings. The highest occupied molecular orbital (HOMO) and HOMO-1 are totally concentrated on the carbazole unit of the attaching 3,6-(di-*tert*-butylcarbazol-*N*-yl)octyl moieties, whereas the conjugated backbone of 4-(7-(carbazol-*N*-yl)fluoren-2-yl)-7-(4-(carbazol-*N*-yl)phenyl)benzothiadiazole contributes to both HOMO-2 and HOMO-3 orbitals. HOMO-2 is mainly delocalized on the 4-(7-(carbazol-*N*-yl)fluoren-2-yl)benzothiadiazole segment and HOMO-3 is largely distributed on the 7-(4-(carbazol-*N*-yl)phenyl)benzothiadiazole part. Deliberately, such orbital characteristics, in general, can improve the orbital coupling interaction and retain the CT transition of the conjugated backbone in the excited state. Particularly, the separation of the HOMO-2/HOMO-3 and LUMO suggests a CT-like character, while the fractional overlap of the HOMO-2/HOMO-3 and LUMO reveals a LE-like character, leading to a radiative decay rate and thus high PL and EL efficiencies concurrently as the emitter utilized in OLEDs. To further understand the excited-state properties of the molecule, the natural transition orbitals (NTOs) of singlet (S) and triplet (T) excited states to explore the electron transition properties were performed based on time-dependent (TD)-DFT using the B3LYP/6-31G(d,p) function.[59] As shown in Fig. 3b, the hole and particle of **CPBzFC** mainly look like its HOMO-2/HOMO-3 and LUMO orbitals, respectively, with more electron distributions in the Bz unit of the hole as a result of the lessened twist angles along the conjugated backbone in the excited state. The transitions of $S_0 \rightarrow S_1$ and $S_0 \rightarrow S_4$ visibly unveil the HLCT transition characteristics, in which a significant spatial separation but a certain overlap can be observed between the "hole" and "particle" wave functions. Vitally, the S_1 state ($f = 0.460$) gives a much larger oscillator strength (f) than the S_4 state ($f = 0.044$) owing to a greater overlap of the two wave functions or LE components, which is essential for a high PL efficiency. The NTO analysis of the higher S and T states (Fig. 3c) also revealed that the triplet excitons of **PBzFC** are mainly decayed through $T_2/T_3/T_4 \rightarrow S_1$ transitions, through a "hot exciton"

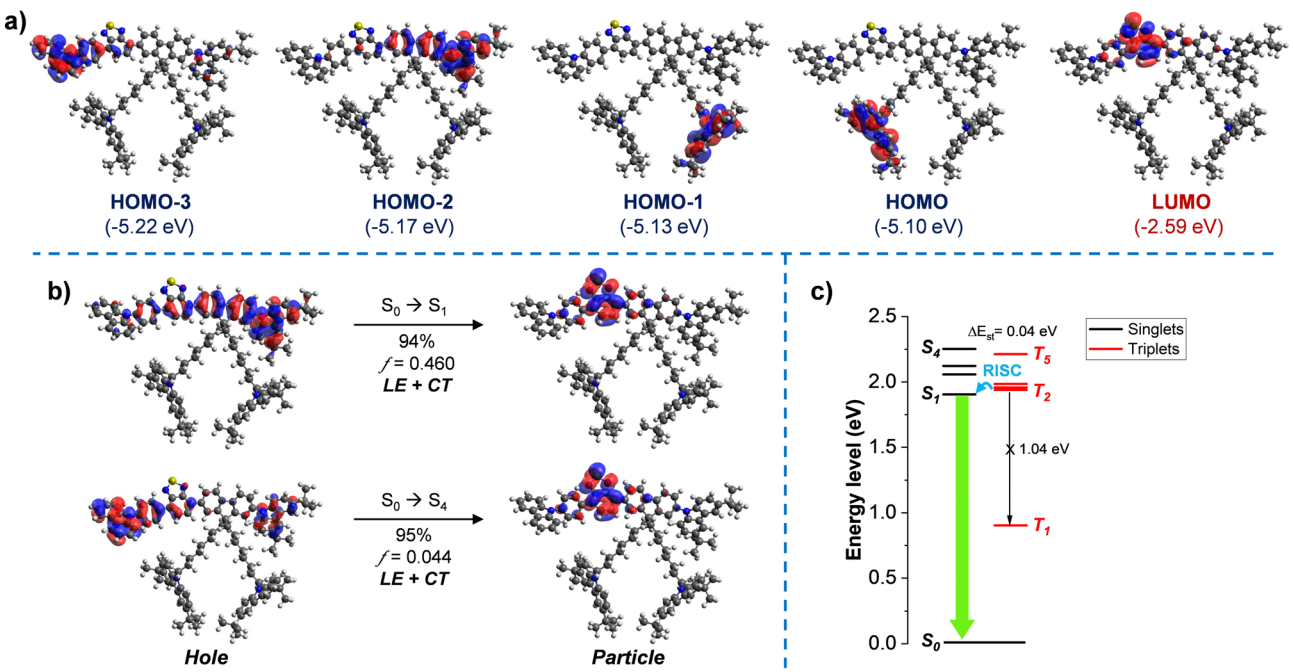

Fig. 3 (a) The optimized structure obtained in the gas phase and HOMO/LUMO distribution calculations using the B3LYP/6-31G(d,p) method. (b) The natural transition orbits (NTOs) of $S_0 \rightarrow S_1$ and $S_0 \rightarrow S_4$ transitions calculated using the TD-B3LYP/6-31G(d,p) function. The percentage is the proportion of transitions. (c) The energy diagram of the singlet (S) and triplet (T) excited states.

reverse intersystem crossing (hRISC) process.[30,60,61] Meanwhile, the energy gap between T_1 and T_2 of 1.04 eV is strong enough to suppress a non-radiative interconversion (IC) transition from T_2 to T_1, ensuing a favorable RISC process of $T_2 \rightarrow S_1$ transition.[62,63] There is also a large ΔE_{ST} ($S_1 - T_1$) (1.01 eV); thus, a RISC process ($T_1 \rightarrow S_1$ transition) *via* the thermally activated delayed fluorescence (TADF) mechanism is considered to be rationally unlikely.[64]

The thermal properties analyzed by thermogravimetric analysis (TGA) and differential scanning calorimetry (DSC) under a nitrogen atmosphere revealed that **PBzFC** was an amorphous material with high thermal stability. The TGA curve exhibited decomposition temperatures at 5% weight loss (T_{5d}) over 421 °C, while the DSC trace displayed a distinct endothermic baseline shift related to a glass transition temperature (T_g) at 147 °C (Fig. 4a and Table 1). The morphology of **PBzFC** thin films prepared by spin coating from its toluene solution was examined by atomic force microscopy (AFM). As shown in Fig. 4b, a tapping-mode AFM image of the thin film exhibited a smooth surface with no pinholes and crystalline islands like an amorphous morphology with a root-mean-square (rms) roughness of 0.408 nm, stating a nanoscale thin film with high quality. The feature of high thermal stability and good film-forming capability of **PBzFC** is useful and necessary for the fabrication of OLED devices by solution-based methods.[65,66]

The electronic properties and redox behavior of **PBzFC** were analyzed by cyclic voltammetry (CV) measurement performed in dichloromethane containing 0.1 M *n*-Bu_4NPF_6 as a supporting electrolyte under an argon atmosphere. As shown in Fig. 4c, the CV plot displays an ambipolar redox feature comprising one quasi-reversible reduction and two oxidation processes (Table 1). The reduction wave occurring at a half-wave potential ($E_{1/2}$) of −1.39 eV could be assigned to the Bz unit reduction.[67,68] The first oxidation wave occurring at an $E_{1/2}$ of 1.15 V could be related to the oxidation of 3,6-di-*tert*-butylcarbazole moiety forming radical cations,[41,42,69] while the second oxidation wave at an $E_{1/2}$ of 1.38 V could be attributed to the oxidation of the π-conjugated 4-(7-(carbazol-*N*-yl)fluoren-2-yl)benzothiadiazole fragment. Additionally, the repeated CV scans exhibited unchanged CV traces implying that **PBzFC** is an electrochemically stable molecule (Fig. S1, ESI†). Based on the onset oxidation (E^{ox}_{onset})/reduction (E^{re}_{onset}) potentials, the electrochemical bandgap (E^{ele}_g) was determined to be 2.41 eV, which is found to be slightly narrower than the optical bandgap (E^{opt}_g = 2.53 eV) estimated from the onset of the absorption spectrum in a thin film.[70] The HOMO level was calculated from E^{ox}_{onset} to be −5.51 eV, and the LUMO level was then deduced from the HOMO and E^{opt}_g to be −2.98 eV (Table 1). Apparently, the 3,6-di-*tert*-butylcarbazole unit of the attaching 3,6-di-*tert*-butylcarbazol-*N*-yl)octyl parts in the molecule contributes to its HOMO level, as observed in the DFT calculation results. Importantly, **PBzFC** retains a low HOMO level, meaning that it could be applied as a hole-transporting layer (HTL)-free emissive material. Because, the HOMO of **PBzFC** matches well with the work function of the ITO/PEDOT:PSS anode (5.10–5.40 eV) (Fig. 5a), signifying that **PBzFC** can be directly fabricated on the top of this electrode without an HTL, allowing the fabrication of a simple structured solution-processed OLED. Because the most demanding task for the solution-processed multilayer OLED fabrication is getting an organic solvent-insoluble HTL material to avoid washing away the HTL during the solution-processed fabrication of emissive materials. Hence, **PBzFC** as an HTL-free fluorophore is an ideal emissive material for solution-processed OLEDs. The hole-transporting properties of **PBzFC** in thin films were then evaluated using the hole-only device (HOD) with the configuration of ITO/PEDOT:PSS/**PBzFC** (100 nm)/MoO_3/Al, where molybdenum trioxide (MoO_3) will serve as the hole injection layer to block electrons from the opposite electrode, while a thick layer of **PBzFC** will help to avoid charge-carrier accumulation.[71–73] According to the space-charge-limited current (SCLC) theory, the hole mobility can be calculated from the current density–voltage (*J*–*V*) plot of the HOD (Fig. 4d). By combining the Mott–Gurney equation and the Frenkel effect,[74] the hole mobility of **PBzFC** is estimated to be 7.54×10^{-7} cm^2 V^{-1} s^{-1}.

Inspired by its high Φ_{PL} and solution-processed HTL-free emissive feature, the electroluminescence (EL) properties of **PBzFC** as a non-doped emitter for the simple solution-processed OLED was evaluated with the device configuration of ITO/PEDOT:PSS:Nf (40 nm)/**PBzFC** (35 nm)/TPBi (40 nm)/LiF (1 nm)/Al (100 nm) (Fig. 5a). In this device, indium tin oxide (ITO) and aluminum (Al) are the electrodes, lithium fluoride (LiF) is an electron injection layer, 1,3,5-tri(1-phenyl-1*H*-benzo[*d*]imidazol-2-yl)phenyl (TPBi) acts as both the electron transport layer and hole blocking layer, and Nafion® perfluorinated

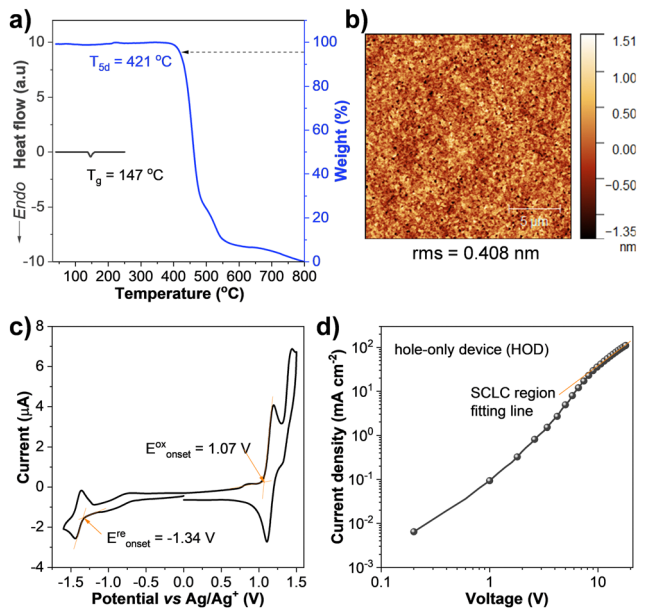

Fig. 4 (a) DSC and TGA thermograms studied at a heating rate of 10 °C min under a N_2 flow. (b) AFM images of the thin film. (c) Cyclic voltammograms measured in dry CH_2Cl_2 solution scanned at a rate of 50 mV s^{-1} under Ar. (d) The current density–voltage (*J*–*V*) plot of the hole-only device.

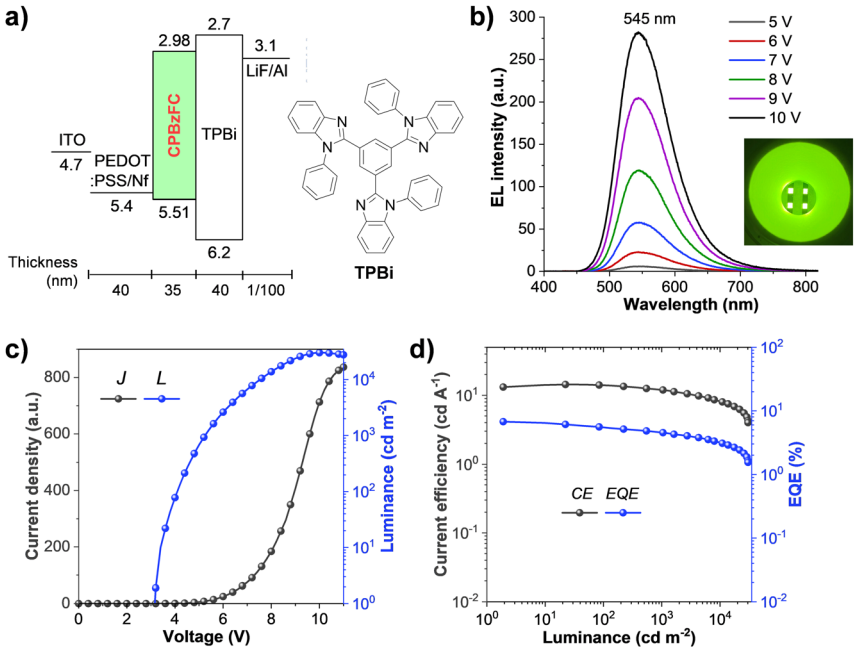

Fig. 5 (a) Device structure and energy levels (relative to the vacuum energy level) and the molecular structure of the organic material used. (b) EL spectra at various applied voltages (inset: photograph of the glowing OLED device). (c) Current density–voltage–luminance (*J*–*V*–*L*) characteristics and (d) current efficiency–current density–EQE (CE–*J*–EQE) plots.

resin (Nf) doped poly(3,4-ethylenedioxythiophene):poly(4-styrene sulfonate) (PEDOT:PSS) (PEDOT:PSS:Nf) is utilized as a hole injection layer. The gradient work function of this PEDOT:PSS:Nafion® mixed film from −5.10 to −5.45 eV and then 5.61 eV fits well with both the work function of the ITO (4.7 eV) anode and the HOMO level of the **PBzFC** emissive layer.[75,76] This would not only reduce the energy barrier between the two layers but also enhance the hole injection at the interfaces into the device, giving rise to a low turn-on voltage. The results of the EL characteristics and performances of this device are displayed in Fig. 4 (Table 2). The solution-processed OLED showed a low turn-on voltage (a luminance of 1 cd m^{-2}) of 3.2 V, indicating the efficient charge injection and transporting properties in the device. As illustrated in Fig. 5b, the OLED exhibits a strong yellowish-green emission peaked at 545 nm, which is close to its PL peak in the neat films (550 nm), and the Commission Internationale de L'Eclairage (CIE) coordinates (*x*, *y*) of (0.39, 0.57). Moreover, these EL spectra were unchanged under varying applied voltages with no emissions from the excimer and the exciplex at the EML/TPBi interface, suggesting the satisfied device stability during the electrical charge injection process. This simple structured **PBzFC**-based OLED delivered an excellent EL performance with an ultrahigh brightness of (L_{max}) of 30 800 cd m^{-2}, a maximum external quantum efficiency (EQE_{max}) of 6.74%, a maximum current efficiency (CE_{max}) of 14.38 cd A^{-1}, and a maximum power efficiency (PE_{max}) of 13.06 lm W^{-1} (Table 2). Furthermore, the efficiency roll-off of this device is rather small and can continue to retain a relatively decent efficiency at high brightness. For example, its EQE can maintain 4.52% at a practicable brightness of 1000 cd m^{-2} and 3.20% even at a brightness of 10 000 cd m^{-2}. However, the decrease in the efficiency of this OLED at every high brightness could be accountable to its simple-structured device, which could cause the leak of the charge from the emissive layer, and an imperfect charge carrier balance in the device.[77,78] Comprehensively, this **PBzFC**-based bilayer device performance represents one of the best results of solution-processed HLCT-based OLEDs reported to date (Table S1, ESI†),[36–39,79] and is comparable to the EL performance of the thermal evaporated multiple layered OLED of its paternal HLCT molecule 4-(4-(carbazol-9-yl)phenyl)-7-phenylbenzothiadiazole (CzP-BZP) (EQE_{max} = 6.95%).[25] To further study the utilization of excitons in the EL process, the exciton utilization efficiency (EUE) was calculated using EUE = EQE/($\eta_{out} \times \eta_{rec} \times \Phi_{PL}$),[80–82]

Table 2 Electroluminescence data of the fabricated solution-processed OLED[a]

				EQE/CE/PE[b] (%, cd A^{-1}, lm W^{-1})				
V_{on} (V)	λ_{EL} (nm)	J_{max} (mA cm^{-2})	L_{max} (cd m^{-2})	Maximum	@1000 cd m^{-2}	@10 000 cd m^{-2}	CIE (*x*, *y*)	EUE[c] (%)
3.2	545	712	30 300	6.74/14.38/13.06	4.52/11.96/7.28	3.20/8.31/3.52	0.39, 0.57	41

[a] ITO/PEDOT:PSS:Nf (40 nm)/**CPBzFC** (35 nm)/TPBi (40 nm)/LiF (1 nm):Al (100 nm). [b] External quantum efficiency/current efficiency/power efficiency. [c] Singlet exciton utilization efficiency.

where η_{out} is the light outcoupling efficiency which is roughly 20% for glass substrates, Φ_{PL} is the absolute PL quantum yield of the emissive layer in a thin film (Φ_{PL} = 82%), and η_{rec} is the fraction of the exciton formation of the injected charge carriers and it is 100% for ideal charge recombination. Accordingly, the EUE was determined to be 41%. Hence, the radiative exciton yield of this device surpassed 25% of the conventional fluorescent OLEDs, confirming that **PBzFC** is an efficient solution-processed HLCT emitter. Even so, its EQE is modest in comparison to those of the reported state-of-the-art multi-layer thermally evaporated HLCT-based OLEDs; this device offers a simple non-doped device architecture (only two solution-processed organic layers) with a low-cost fabrication process, which is desirable for practical usage.

Experimental

Materials and methods

All commercially available reagents were purchased and used as received. ^{1}H NMR and ^{13}C NMR spectra were recorded using a Bruker Avance III HD 600 MHz NMR spectrometer with tetramethylsilane as the internal standard and chloroform-*d* as the solvent. High-resolution mass spectra (HRMS) were acquired using either a Bruker Autoflex Speed MALDI TOF/TOF mass spectrometer or a LC-Quadrupole-Time-of Flight Tandem mass spectrometer. Thermogravimetric analysis (TGA) and differential scanning calorimetry (DSC) measurements were carried out under a N_2 flow at a heating rate of 10 °C min^{-1} using a Rigaku Thermo plus EVO2 and PerkinElmer double-furnace DSC 8500. Electrochemical analyses were performed using an Autolab potentiostat PGSTA101 with a three-electrode system (glassy carbon as the working electrode, Pt as the counter electrode, and Ag/AgCl as the reference electrode) in dry CH_2Cl_2 containing 0.1 M *n*-Bu_4NPF_6 as a supporting electrolyte under an argon atmosphere at a scan rate of 50 mV s^{-1}. The thin-film morphology was analyzed using a Park NX10 AFM operated in the non-contact mode under the ambient conditions. UV-vis absorption spectra were measured in solutions and thin films coated on quartz substrates using a PerkinElmer LAMBDA 1050 spectrophotometer. Photoluminescence (PL) spectra and PL decay profiles were recorded using an Edinburgh Instruments FLS980 spectrometer. The absolute photoluminescence quantum yields (Φ_{PL}) were recorded using an Edinburgh Instruments FLS980 spectrometer integrated with a calibrated integrating sphere. Melting points were measured using a Krüss KSP1N melting point meter and the data were uncorrected.

The density functional theory (DFT) calculations were performed using Gaussian 16 software.[83] The ground state geometries, HOMO/LUMO distributions, and HOMO/LUMO energy levels were computed and completely optimized by the B3LYP/6-31G(d) level of theory in the gas phase. The natural transition orbitals (NTOs) calculations of singlet (S) and triplet (T) excited states were then performed based on time-dependent (TD)-DFT using the B3LYP/6-31G(d,p) function.

Device fabrication and testing

The double-layered solution-processed OLED device using **CPBzFC** as an emissive layer (EML) with the optimized configuration of ITO/PEDOT:PSS:Nf (40 nm)/EML (35 nm)/TPBi (40 nm)/LiF (1 nm)/Al (100 nm) was fabricated and assessed as follows. The indium tin oxide (ITO) glass substrate with a sheet resistance of 12 Ω sq^{-1} was cleaned with Liquinox™, deionized water, acetone, and isopropyl alcohol, respectively. The substrate was flushed with N_2 gas and surface-treated with UV-ozone for 20 min. The substrate was then spin-coated on top with a hole injection layer (HIL) of Nafion® perfluorinated resin (Nf) doped poly(3,4-ethylenedioxythiophene):poly(4-styrene sulfonate (PEDOT:PSS) (PEDOS:PSS:Nf) at a spin speed of 5000 rpm for 30 seconds and dried at 120 °C for 30 min. After this, the toluene solution of EML (2% w/v) was spin-coated on top of the HIL at a spin speed of 3000 rpm for 30 seconds and heated at 80 °C for 30 min. The thicknesses of all spin-coated films were measured using a Dektak XTL stylus profilometer. The coated substrates were then transferred to a vacuum deposition system at a base pressure lower than 5×10^{-6} Pa for organic and metal depositions. The layers of 1,3,5-tri(1-phenyl-1*H*-benzo[*d*]imidazol-2-yl)phenyl (TPBi) as both the electron transport layer and the hole blocking layer, LiF as an electron injecting layer (EIL), and aluminum as the cathode were thermally evaporated using a Kurt J. Lasker mini SPECTROS 100 thin-film deposition system to form an active area of 4 mm^2. The film thickness was monitored and controlled using a quartz crystal microbalance (QCM) integrated with the instrument. All devices were measured and analyzed using a Keithley 2400 source meter, a Hamamatsu Photonics PMA-12 multichannel analyzer, and an integrating sphere equipped with a Hamamatsu photonics C9920-12 external quantum efficiency (EQE) measurement system under an ambient condition.

Synthesis and characterization

4-(4-(Carbazol-*N*-yl)phenyl)-7-(4,4,5,5-tetramethyl-1,3,2-dioxaborolan-2-yl)benzothiadiazole (3). A mixture of **2** (0.70 g, 1.53 mmol), bis(pinacolato)diboron (0.97 g, 3.83 mmol), KOAc (0.75 g, 7.7 mmol), and $Pd(dppf)_2Cl_2$ (65 mg, 0.08 mmol) in dried toluene (45 mL) was degassed with N_2 for 15 min. It was stirred under reflux for 16 h. After being cooled to room temperature, it was filtered through Celite and eluted with CH_2Cl_2. The solvent was removed to dryness. The crude was purified by column chromatography on silica gel eluting with CH_2Cl_2 : hexane (1 : 4) to give yellow solids (0.52 g, 67%). ^{1}H NMR (600 MHz, $CDCl_3$) δ 8.32 (d, J = 6.8 Hz, 1H), 8.23 (d, J = 8.3 Hz, 2H), 8.17 (d, J = 7.7 Hz, 2H), 7.76 (d, J = 8.3 Hz, 2H), 7.55 (d, J = 8.2 Hz, 2H), 7.44 (t, J = 7.6 Hz, 2H), 7.31 (t, J = 7.4 Hz, 2H), 1.48 (s, 12H); ^{13}C NMR (151 MHz, $CDCl_3$) δ 140.76, 139.08, 130.88, 127.34, 127.05, 126.04, 123.57, 120.36, 120.14, 109.95, 84.46, 24.95; HRMS MALDI-TOF (*m*/*z*) calcd for $C_{30}H_{26}BN_3O_2S$: 503.1839; found: 503.0446 [M^+].

9,9′-((2-Bromo-7-(3,6-di-*tert*-butylcarbazol-*N*-yl)-fluorene-9,9-diyl)bis(octane-8,1-diyl))bis(3,6-di-*tert*-butylcarbazole) (7). A mixture of 3,6-di-*tert*-butylcarbazole (0.33 g, 1.20 mmol), 6 (2.91 g,

2.64 mmol), CuI (0.23 g, 1.20 mmol), K_3PO_4 (1.27 g, 5.99 mmol), and (±)-*trans*-1,2-diaminocyclohexane (0.3 mL) in toluene (15 mL) was degassed with N_2 for 5 min and then heated at reflux under a N_2 atmosphere for 24 h. After being cooled to room temperature, it was filtered through a plug of silica eluting with CH_2Cl_2. The solvent was removed to dryness. The crude was purified by column chromatography on silica gel eluting with CH_2Cl_2 : hexane (1 : 4) to give white solids (1.25 g, 81%). ^{1}H NMR (600 MHz, $CDCl_3$) δ 8.17 (s, 2H), 8.08 (s, 4H), 7.81 (d, J = 7.7 Hz, 1H), 7.57 (d, J = 8.2 Hz, 1H), 7.53–7.43 (m, 10H), 7.37 (d, J = 8.6 Hz, 2H), 7.22 (d, J = 8.5 Hz, 4H), 4.15 (t, J = 7.0 Hz, 4H), 1.99–1.90 (m, 4H), 1.80–1.70 (m, 4H), 1.48–1.43 (m, 54H), 1.33–1.25 (m, 4H), 1.20–1.14 (m, 4H), 1.12–1.02 (m, 8H), 0.77–0.63 (m, 4H); ^{13}C NMR (151 MHz, $CDCl_3$) δ 153.04, 151.98, 142.91, 141.34, 139.47, 139.24, 138.93, 138.77, 137.31, 130.23, 126.22, 125.49, 123.57, 123.43, 123.15, 122.62, 121.27, 121.17, 120.89, 116.37, 116.20, 109.13, 107.96, 55.63, 43.10, 40.14, 34.75, 34.62, 32.06, 32.03, 29.81, 29.28, 29.12, 29.07, 27.24, 23.79; HRMS MALDI-TOF m/z calcd for $C_{89}H_{110}N_3Br$: 1301.7840; found: 1221.9532 [M–Br$^+$].

CPBzFC. A mixture of 7 (200 mg, 0.15 mmol), 3 (50 mg, 0.10 mmol), 10% K_2CO_3 (aq) (5 mL) and $Pd(PPh_3)_4$ (6 mg, 0.005 mmol) in dried THF (25 mL) was degassed with N_2 for 10 min. It was stirred and heated to reflux under a N_2 atmosphere for 12 h. After being cooled to room temperature, water (50 mL) was added followed by extraction with CH_2Cl_2 (3 × 50 mL). The combined organic layer was washed with water (50 mL), brine solution (50 mL), dried over anhydrous Na_2SO_4, filtered, and concentrated *in vacuo* to dryness. The crude was purified by column chromatography on silica gel eluting with CH_2Cl_2 : hexane (1 : 4) to give yellow solids (94 mg, 59%). M.p. = 180–181 °C. ^{1}H NMR (600 MHz, $CDCl_3$) δ 8.22 (d, J = 8.0 Hz, 2H), 8.18 (d, J = 7.8 Hz, 4H), 8.07–8.01 (m, 6H), 7.95–7.87 (m, 4H), 7.77 (d, J = 8.0 Hz, 2H), 7.59–7.54 (m, 4H), 7.50–7.38 (m, 10H), 7.32 (t, J = 7.4 Hz, 2H), 7.18 (d, J = 8.6 Hz, 4H), 4.11 (t, J = 7.3 Hz, 4H), 2.13–1.98 (m, 4H), 1.72 (q, J = 7.6 Hz, 4H), 1.47 (s, 18H), 1.40 (s, 36H), 1.32–1.23 (m, 4H), 1.22–1.06 (m, 12H), 0.85 (s, 4H); ^{13}C NMR (151 MHz, $CDCl_3$) δ 154.3, 154.1, 152.9, 151.2, 142.9, 141.3, 140.8, 140.8, 139.3, 138.9, 137.8, 137.2, 136.4, 136.2, 134.1, 132.1, 130.7, 128.3, 127.9, 127.1, 126.0, 124.0, 123.6, 123.5, 123.4, 123.1, 122.6, 120.4, 120.1, 119.9, 116.4, 116.2, 110.0, 109.2, 107.9, 55.6, 43.1, 40.3, 34.8, 34.6, 32.1, 30.0, 29.3, 29.2, 29.1, 27.2, 24.0; HRMS MALDI-TOF (m/z) calcd for $C_{113}H_{124}N_6S$: 1597.9642; found: 1597.4173 [M$^+$].

Conclusions

In conclusion, a solution-processed fluorophore (CPBzFC) with the HLCT character was structurally developed by connecting 7-(4-(carbazol-*N*-yl)phenyl)benzothiadiazole HLCT part to a hole-transporting and highly soluble 7-(3,6-di-*tert*-butylcarbazol-*N*-yl)-9,9′-bis(8-(3,6-di-*tert*-butylcarbazol-*N*-yl)octyl)fluorene moiety. CPBzFC implemented an appropriate twisted D–A conformation allowing both the locally excited (LE) and charge transfer (CT) states to coexist with energetic closeness. CPBzFC showed an intense yellowish-green fluorescence color at 550 nm with a high solid-state fluorescence quantum yield of 82%. The solvatochromic and theoretical findings verified that CPBzFC retained an HLCT feature. This molecule exhibited high thermal stability with a good film-forming quality, shallow HOMO level (−5.51 eV), and decent hole mobility. It was effectively utilized as a hole-transporting-layer-free non-doped emissive layer in a simple structured solution-processed OLED, which accomplished an excellent device performance with a high brightness of 30 800 cd m^{-2}, a maximum external quantum efficiency (EQE_{max})of 6.74%, a maximum current efficiency (CE_{max}) of 14.38 cd A^{-1}, and a high EUE of 41%, which is as good as the EL performance of its paternal HLCT molecule 4-(4-(carbazol-9-yl)phenyl)-7-phenylbenzothiadiazole (CzP-BZP)-based thermal evaporated multiple layered OLED (EQE_{max} = 6.95%). These findings present a useful design approach for constructing an efficient solution-processed HLCT emitter for high efficiency simple-structured non-doped OLEDs and this will be a helpful example for the further development of new HLCT materials, enabling the progress of next-generation OLEDs.

Author contributions

T. L. performed the materials synthesis and characterization and device fabrication, discussed the data, and prepared the original draft. P. C. performed the quantum chemical calculations and analyzed the data. S. P., N. C., P. T., W. W., and T. W. partially performed the materials synthesis and characterization and device fabrication and analyzed the data. V. P. conceived and supervised the project and reviewed and edited the final draft. All the authors approved the final version of the manuscript.

Conflicts of interest

There are no conflicts to declare.

Acknowledgements

This work was funded by the National Research Council of Thailand (NRCT) (no. N42A650196) and the National Nanotechnology Center (Nanotec), the National Science and Technology Development Agency, Ministry of Higher Education, Science, Research and Innovation, Thailand, through its program of Research Network National Nanotechnology Center. We also acknowledged the Postdoctoral Fellowship (to T. S.) from VISTEC.

Notes and references

1 C. W. Tang and S. A. Vanslyke, Organic electroluminescent diodes, *Appl. Phys. Lett.*, 1987, **51**, 913–915.
2 C. Adachi and A. S. D. Sandanayaka, The leap from organic light-emitting diodes to organic semiconductor laser diodes, *CCS Chem.*, 2020, **2**, 1203–1216.

3 J. Kumsampao, C. Chaiwai, C. Sukpattanacharoen, P. Nalaoh, T. Chawanpunyawat, P. Chasing, S. Namuangruk, N. Kungwan, T. Sudyoadsuk and V. Promarak, Solid-state fluorophores with combined excited-state intramolecular proton transfer-aggregation-induced emission as efficient emitters for electroluminescent devices, *Adv. Photonics Res.*, 2022, **3**, 2100141.
4 Y. Xu, P. Xu, D. Hu and Y. Ma, Recent progress in hot exciton materials for organic light-emitting diodes, *Chem. Soc. Rev.*, 2021, **50**, 1030–1069.
5 P. Therdkatanyuphong, P. Chasing, C. Kaiyasuan, S. Boonnab, T. Sudyoadsuk and V. Promarak, High solid-state near infrared emissive organic fluorophores from thiadiazole[3,4-c]pyridine derivatives for efficient simple solution-processed nondoped near infrared OLEDs, *Adv. Funct. Mater.*, 2020, **30**, 2002481.
6 H. W. Chen, J. H. Lee, B. Y. Lin, S. Chen and S. T. Wu, Liquid crystal display and organic light-emitting diode display: present status and future perspectives, *Light: Sci. Appl.*, 2018, **7**, 17168.
7 D. H. Ahn, S. W. Kim, H. Lee, I. J. Ko, D. Karthik, J. Y. Lee and J. H. Kwon, Highly efficient blue thermally activated delayed fluorescence emitters based on symmetrical and rigid oxygen-bridged boron acceptors, *Nat. Photonics*, 2019, **13**, 540–546.
8 P. Tao, Y. Miao, H. Wang, B. Xu and Q. Zhao, High-performance organic electroluminescence: design from organic light-emitting materials to devices, *Chem. Rec.*, 2019, **19**, 1531–1561.
9 S. Reineke, F. Lindner, G. Schwartz, N. Seidler, K. Walzer, B. Lüssem and K. Leo, White organic light-emitting diodes with fluorescent tube efficienc, *Nature*, 2009, **459**, 234–238.
10 W. Zeng, H. Y. Lai, W. K. Lee, M. Jiao, Y. J. Shiu, C. Zhong, S. Gong, T. Zhou, G. Xie, M. Sarma, K. T. Wong, C. C. Wu and C. Yang, Achieving nearly 30% external quantum efficiency for orange–red organic light emitting diodes by employing thermally activated delayed fluorescence emitters composed of 1,8-naphthalimide-acridine hybrids, *Adv. Mater.*, 2018, **30**, 1704961.
11 J. Kumsampao, C. Chaiwai, P. Chasing, T. Chawanpunyawat, S. Namuangruk, T. Sudyoadsuk and V. Promarak, A simple and strong electron-deficient 5,6-dicyano[2,1,3]benzothiadiazole-cored donor-acceptor-donor compound for efficient near infrared thermally activated delayed fluorescence, *Chem. – Asian J.*, 2020, **15**, 3029–3036.
12 T. L. Wu, M. J. Huang, C. C. Lin, P. Y. Huang, T. Y. Chou, R. W. Chen-Cheng, H. W. Lin, R. S. Liu and C. H. Cheng, Diboron compound-based organic light-emitting diodes with high efficiency and reduced efficiency roll-off, *Nat. Photonics*, 2018, **12**, 235–240.
13 Y. Pan, W. Li, S. Zhang, L. Yao, C. Gu, H. Xu, B. Yang and Y. Ma, High yields of singlet excitons in organic electroluminescence through two paths of cold and hot excitons, *Adv. Opt. Mater.*, 2014, **2**, 510–515.
14 J. Zhang, Y. Zhao, H. Xu, D. Zhang, Y. Miao, R. Shinar, J. Shinar, H. Wang, B. Xu and Y. Wu, Novel blue fluorescent emitters structured by linking triphenylamine and anthracene derivatives for organic light-emitting devices with EQE exceeding 5%, *J. Mater. Chem. C*, 2019, **7**, 10810–10817.
15 W. Li, Y. Pan, L. Yao, H. Liu, S. Zhang, C. Wang, F. Shen, P. Lu, B. Yang and Y. Ma, A hybridized local and charge-transfer excited state for highly efficient fluorescent OLEDs: molecular design, spectral character, and full exciton utilization, *Adv. Opt. Mater.*, 2014, **2**, 892–901.
16 X. Lv, M. Sun, L. Xu, R. Wang, H. Zhou, Y. Pan, S. Zhang, Q. Sun, S. Xue and W. Yang, Highly efficient non-doped blue fluorescent OLEDs with low efficiency roll-off based on hybridized local and charge transfer excited state emitters, *Chem. Sci.*, 2020, 5058–5065.
17 Y. Liu, H. Liu, Q. Bai, C. Du, A. Shang, D. Jiang, X. Tang and P. Lu, Pyrene[4,5- d]imidazole-based derivatives with hybridized local and charge-transfer state for highly efficient blue and white organic light-emitting diodes with low efficiency roll-off, *ACS Appl. Mater. Interfaces*, 2020, **12**, 16715–16725.
18 J. Tagare and S. Vaidyanathan, Recent development of phenanthroimidazole-based fluorophores for blue organic light-emitting diodes (OLEDs): an overview, *J. Mater. Chem. C*, 2018, **6**, 10138–10173.
19 W. Li, D. Liu, F. Shen, D. Ma, Z. Wang, T. Feng, Y. Xu, B. Yang and Y. Ma, A twisting donor-acceptor molecule with an intercrossed excited state for highly efficient, deep-blue electroluminescence, *Adv. Funct. Mater.*, 2012, **22**, 2797–2803.
20 Z. Huang, B. Wang, Q. Zhang, S. Xiang, X. Lv, L. Ma, B. Yang, Y. Gao and L. Wang, Highly twisted bipolar emitter for efficient nondoped deep-blue electroluminescence, *Dyes Pigm.*, 2017, **140**, 328–336.
21 Y. Xu, X. Liang, X. Zhou, P. Yuan, J. Zhou, C. Wang, B. Li, D. Hu, X. Qiao, X. Jiang, L. Liu, S. J. Su, D. Ma and Y. Ma, Highly efficient blue fluorescent OLEDs based on upper level triplet–singlet intersystem crossing, *Adv. Mater.*, 2019, **31**, 1807388.
22 Y. Tan, Z. Zhao, L. Shang, Y. Liu, C. Wei, J. Li, H. Wei, Z. Liu, Z. Bian and C. Huang, A novel bipolar D-π-A type phenanthroimidazole/carbazole hybrid material for high efficiency nondoped deep-blue organic light-emitting diodes with NTSC CIE:Y and low efficiency roll-off, *J. Mater. Chem. C*, 2017, **5**, 11901–11909.
23 S. Xiao, S. T. Zhang, Y. Gao, X. Yang, H. Liu, W. Li and B. Yang, Efficient and stable deep-blue narrow-spectrum electroluminescence based on hybridized local and charge-transfer (HLCT) state, *Dyes Pigm.*, 2021, **193**, 109482.
24 S. Xiao, Y. Gao, R. Wang, H. Liu, W. Li, C. Zhou, S. Xue, S. T. Zhang, B. Yang and Y. Ma, Highly efficient hybridized local and Charge-transfer (HLCT) Deep-blue electroluminescence with excellent molecular horizontal orientation, *Chem. Eng. J.*, 2022, **440**, 135911.
25 C. Wang, X. Li, Y. Pan, S. Zhang, L. Yao, Q. Bai, W. Li, P. Lu, B. Yang, S. Su and Y. Ma, Highly efficient nondoped green organic light-emitting diodes with combination of high photoluminescence and high exciton utilization, *ACS Appl. Mater. Interfaces*, 2016, **8**, 3041–3049.
26 W. Xie, B. Li, X. Cai, M. Li, Z. Qiao, X. Tang, K. Liu, C. Gu, Y. Ma and S. J. Su, Thiophene disubstituted benzothiadiazole derivatives: An effective planarization strategy toward

deep-red to near-infrared (NIR) organic light-emitting diodes, *Front. Chem.*, 2019, **7**, 276.

27 X. Chen, Z. Yang, W. Li, Z. Mao, J. Zhao, Y. Zhang, Y. C. Wu, S. Jiao, Y. Liu and Z. Chi, Nondoped red fluorophores with hybridized local and charge-transfer state for high-performance fluorescent white organic light-emitting diodes, *ACS Appl. Mater. Interfaces*, 2019, **11**, 39026–39034.

28 Q. Luo, C. Lv, H. Sheng, F. Cao, J. Sun, C. Zhang, M. Ouyang, B. Zou and Y. Zhang, Highly bright fluorescence from dispersed dimers: deep-red polymorphs and wide-range piezochromism, *Adv. Opt. Mater.*, 2020, **8**, 1901836.

29 X. Chen, D. Ma, T. Liu, Z. Chen, Z. Yang, J. Zhao, Z. Yang, Y. Zhang and Z. Chi, Hybridized local and charge-transfer excited state fluorophores through regulation of donor-acceptor torsion angle for highly-efficient OLEDs, *CCS Chem.*, 2022, **4**, 1284–1294.

30 W. Li, Y. Pan, R. Xiao, Q. Peng, S. Zhang, D. Ma, F. Li, F. Shen, Y. Wang, B. Yang and Y. Ma, Employing ~100% excitons in OLEDs by utilizing a fluorescent molecule with hybridized local and charge-transfer excited state, *Adv. Funct. Mater.*, 2014, **24**, 1609–1614.

31 X. Tang, X. L. Li, H. Liu, Y. Gao, Y. Shen, S. Zhang, P. Lu, B. Yang, S. J. Su and Y. Ma, Efficient near-infrared emission based on donor-acceptor molecular architecture: The role of ancillary acceptor of cyanophenyl, *Dyes Pigm.*, 2018, **149**, 430–436.

32 Q. Wan, J. Tong, B. Zhang, Y. Li, Z. Wang and B. Z. Tang, Exploration of high efficiency AIE-active deep/near-infrared red emitters in OLEDs with high-radiance, *Adv. Opt. Mater.*, 2020, **8**, 1901520.

33 C. Wang, X. L. Li, Y. Gao, L. Wang, S. Zhang, L. Zhao, P. Lu, B. Yang, S. J. Su and Y. Ma, Efficient near-infrared (NIR) organic light-emitting diodes based on donor–acceptor architecture: an improved emissive state from mixing to hybridization, *Adv. Opt. Mater.*, 2017, **5**, 1700441.

34 T. Liu, L. Zhu, S. Gong, C. Zhong, G. Xie, E. Mao, J. Fang, D. Ma and C. Yang, A red fluorescent emitter with a simultaneous hybrid local and charge transfer excited state and aggregation-induced emission for high-efficiency, low efficiency roll-off OLEDs, *Adv. Opt. Mater.*, 2017, **5**, 1700145.

35 Y. Li, J. Yao, C. Wang, X. Zhou, Y. Xu, M. Hanif, X. Qiu, D. Hu, D. Ma and Y. Ma, Highly efficient deep-red/near-infrared D-A chromophores based on naphthothiadiazole for OLEDs applications, *Dyes Pigm.*, 2020, **173**, 107960.

36 H. Usta, D. Alimli, R. Ozdemir, E. Tekin, F. Alkan, R. Kacar, A. G. Altas, S. Dabak, A. G. Gürek, E. Mutlugun, A. F. Yazici and A. Can, A hybridized local and charge transfer excited state for solution-processed non-doped green electroluminescence based on oligo(: p -phenyleneethynylene), *J. Mater. Chem. C*, 2020, **8**, 8047–8060.

37 T. Sudyoadsuk, S. Petdee, P. Chasing, P. Therdkatanyuphong, C. Kaiyasuan, W. Waengdongbung, S. Namuangruk and V. Promarak, A solution-processable hybridized local and charge-transfer (HLCT) phenanthroimidazole as a deep-blue emitter for efficient solution-processed non-doped electroluminescence device, *Dyes Pigm.*, 2021, **195**, 109712.

38 T. Liu, X. Chen, J. Zhao, W. Wei, Z. Mao, W. Wu, S. Jiao, Y. Liu, Z. Yang and Z. Chi, Hybridized local and charge-transfer excited state fluorophores enabling organic light-emitting diodes with record high efficiencies close to 20%, *Chem. Sci.*, 2021, **12**, 5171–5176.

39 Y. Bai, L. Hong, T. Lei, L. Zhang, X. Ouyang, Z. Liu, Y. Chen, W. Li and Z. Ge, Solution-processable, single-layer, blue organic light-emitting diodes employing dual emitting cores of hybridized local and charge-transfer units, *Dyes Pigm.*, 2016, **132**, 94–102.

40 B. Liu, Z. W. Yu, D. He, Z. L. Zhu, J. Zheng, Y. D. Yu, W. F. Xie, Q. X. Tong and C. S. Lee, Ambipolar D-A type bifunctional materials with hybridized local and charge-transfer excited state for high performance electroluminescence with EQE of 7.20% and CIE: Y ~ 0.06, *J. Mater. Chem. C*, 2017, **5**, 5402–5410.

41 C. Poriel and J. Rault-Berthelot, Blue Single-Layer Organic Light-Emitting Diodes Using Fluorescent Materials: A Molecular Design View Point, *Adv. Funct. Mater.*, 2020, **30**, 1910040.

42 W. Kitisriworaphan, T. Chawanpunyawat, T. Manyum, P. Chasing, S. Namuangruk, T. Sudyoadsuk and V. Promarak, The improvement in hole-transporting and electroluminescent properties of diketopyrrolopyrrole pigment by grafting with carbazole dendrons, *RSC Adv.*, 2021, **11**, 12710–12719.

43 P. Khammultri, P. Chasing, C. Chitpakdee, S. Namuangruk, T. Sudyoadsuk and V. Promarak, Red to orange thermally activated delayed fluorescence polymers based on 2-(4-(diphenylamino)-phenyl)-9H-thioxanthen-9-one-10,10-dioxide for efficient solution-processed OLEDs, *RSC Adv.*, 2021, **11**, 24794–24806.

44 G. D. Sharma, M. Anil Reddy, D. V. Ramana and M. Chandrasekharam, A novel carbazole-phenothiazine dyad small molecule as a non-fullerene electron acceptor for polymer bulk heterojunction solar cells, *RSC Adv.*, 2014, **4**, 33279–33285.

45 M. S. Najare, M. K. Patil, T. S. Tilakraj, M. Yaseen, A. Q. A. Nadaf, S. Mantur, S. R. Inamdar and I. A. M. Khazi, Photophysical and electrochemical properties of highly π-conjugated bipolar carbazole-1,3,4-oxadiazole-based d-π-a type of efficient deep blue fluorescent dye, *J. Fluoresc.*, 2021, **31**, 1645–1664.

46 T. M. Clarke, K. C. Gordon, W. M. Kwok, D. L. Phillips and D. L. Officer, Tuning from π,π* to charge-transfer excited states in styryl-substituted terthiophenes: An ultrafast and steady-state emission study, *J. Phys. Chem. A*, 2006, **110**, 7696–7702.

47 H. Detert and V. Schmitt, Quadrupolar donor-acceptor substituted oligo(phenylenevinylene)s - Synthesis and solvatochromism of the fluorescence, *J. Phys. Org. Chem.*, 2004, **17**, 1051–1056.

48 M. Ahn, M. J. Kim, D. W. Cho and K. R. Wee, Electron Push-pull effects on intramolecular charge transfer in perylene-based donor-acceptor compounds, *J. Org. Chem.*, 2021, **86**, 403–413.

49 J. C. Beeson, M. E. Huston, D. A. Pollard, T. K. Venkatachalam and A. W. Czarnik, Structural requirements for efficient photoinduced electron transfer (PET) quenching in 9-aminoalkylanthracenes, *J. Fluoresc.*, 1993, **3**, 65–68.
50 R. M. Duke and T. Gunnlaugsson, Selective fluorescent PET sensing of fluoride (F-) using naphthalimide-thiourea and -urea conjugates, *Tetrahedron Lett.*, 2007, **48**, 8043–8047.
51 M. Hilczer and M. Tachiya, Electric field effects on fluorescence quenching due to electron transfer. II. Linked donor-acceptor systems, *J. Chem. Phys.*, 2002, **117**, 1759–1767.
52 U. Subuddhi, S. Haldar, S. Sankararaman and A. K. Mishra, Photophysical behaviour of 1-(4-N, N-dimethylaminophenylethynyl)pyrene (DMAPEPy) in homogeneous media, *Photochem. Photobiol. Sci.*, 2006, **5**, 459–466.
53 X. Ouyang, X. L. Li, L. Ai, D. Mi, Z. Ge and S. J. Su, Novel ''hot exciton'' blue fluorophores for high performance fluorescent/phosphorescent hybrid white organic light-emitting diodes with superhigh phosphorescent dopant concentration and improved efficiency roll-off, *ACS Appl. Mater. Interfaces*, 2015, **7**, 7869–7877.
54 S. Zhang, W. Li, L. Yao, Y. Pan, F. Shen, R. Xiao, B. Yang and Y. Ma, Enhanced proportion of radiative excitons in non-doped electro-fluorescence generated from an imidazole derivative with an orthogonal donor-acceptor structure, *Chem. Commun.*, 2013, **49**, 11302–11304.
55 H. Laguitton-Pasquier, R. Pansu, J. P. Chauvet, A. Collet, J. Faure and R. Lapouyade, The charge transfer state of excited bianthryl and a derivative: Solvatochromism, emission CT spectra broadening in homogeneous solvents, *Chem. Phys.*, 1996, **212**, 437–455.
56 Z. R. Grabowski, K. Rotkiewicz and W. Rettig, Structural changes accompanying intramolecular electron transfer: focus on twisted intramolecular charge-transfer states and structures, *Chem. Rev.*, 2003, **103**, 3899–4031.
57 X. Lv, M. Sun, L. Xu, R. Wang, H. Zhou, Y. Pan, S. Zhang, Q. Sun, S. Xue and W. Yang, Highly efficient non-doped blue fluorescent OLEDs with low efficiency roll-off based on hybridized local and charge transfer excited state emitters, *Chem. Sci.*, 2020, **11**, 5058–5065.
58 W. Li, P. Chasing, W. Benchaphanthawee, P. Nalaoh, T. Chawanpunyawat, C. Kaiyasuan, N. Kungwan, S. Namuangruk, T. Sudyoadsuk and V. Promarak, Intramolecular hydrogen bond-enhanced electroluminescence performance of hybridized local and charge transfer (HLCT) excited-state blue-emissive materials, *J. Mater. Chem. C*, 2021, **9**, 497–507.
59 R. L. Martin, Natural transition orbitals, *J. Chem. Phys.*, 2003, **118**, 4775–4777.
60 H. Zhang, G. Li, X. Guo, K. Zhang, B. Zhang, X. Guo, Y. Li, J. Fan, Z. Wang, D. Ma and B. Z. Tang, High-performance ultraviolet organic light-emitting diode enabled by high-lying reverse intersystem crossing, *Angew. Chem., Int. Ed.*, 2021, **133**, 22415–22421.
61 D. Chaudhuri, E. Sigmund, A. Meyer, L. Röck, P. Klemm, S. Lautenschlager, A. Schmid, S. R. Yost, T. Vanvoorhis, S. Bange, S. Höger and J. M. Lupton, Metal-free OLED triplet emitters by side-stepping Kasha's rule, *Angew. Chem., Int. Ed.*, 2013, **52**, 13449–13452.
62 L. Yao, S. Zhang, R. Wang, W. Li, F. Shen, B. Yang and Y. Ma, Highly efficient near-infrared organic light-emitting diode based on a butterfly-shaped donor-acceptor chromophore with strong solid-state fluorescence and a large proportion of radiative excitons, *Angew. Chem., Int. Ed.*, 2014, **53**, 2119–2123.
63 Y. Xu, C. Wang, X. Zhou, J. Zhou, X. Guo, X. Liang, D. Hu, F. Li, D. Ma and Y. Ma, Fine modulation of the higher-order excitonic states toward more efficient conversion from upper-level triplet to singlet, *J. Phys. Chem. Lett.*, 2019, **10**, 6878–6884.
64 A. K. Gupta, W. Li, A. Ruseckas, C. Lian, C. L. Carpenter-Warren, D. B. Cordes, A. M. Z. Slawin, D. Jacquemin, I. D. W. Samuel and E. Zysman-Colman, Thermally activated delayed fluorescence emitters with intramolecular proton transfer for high luminance solution-processed organic light-emitting diodes, *ACS Appl. Mater. Interfaces*, 2021, **13**, 15459–15474.
65 H. Xiao, L. Ding, D. Ruan, B. Li, N. Ding and D. Ma, tert-Butylated spirobifluorene derivative incorporating triphenylamine groups: A deep-blue emitter with high thermal stability and good hole transport ability for organic light emitting diode applications, *Dyes Pigm.*, 2015, **121**, 7–12.
66 T. W. Lee, T. Noh, H. W. Shin, O. Kwon, J. J. Park, B. K. Choi, M. S. Kim, D. W. Shin and Y. R. Kim, Characteristics of solution-processed small-molecule organic films and light-emitting diodes compared with their vacuum-deposited counterparts, *Adv. Funct. Mater.*, 2009, **19**, 1625–1630.
67 M. Miranda-Olvera, R. Arcos-Ramos, M. Maldonado-Domínguez, L. Salmon, G. Molnár, A. Bousseksou and M. del Pilar, Carreón-Castro, Design and synthesis of benzothiadiazole-based molecular systems: self-assembly, optical and electronic properties, *New J. Chem.*, 2022, **46**, 4992–5001.
68 X. Chen, D. Ma, T. Liu, Z. Chen, Z. Yang, J. Zhao, Z. Yang, Y. Zhang and Z. Chi, Hybridized local and charge-transfer excited-state fluorophores through the regulation of the donor–acceptor torsional angle for highly efficient organic light-emitting diodes, *CCS Chem.*, 2022, **4**, 1284–1294.
69 G. D. Sharma, M. Anil Reddy, D. V. Ramana and M. Chandrasekharam, A novel carbazole-phenothiazine dyad small molecule as a non-fullerene electron acceptor for polymer bulk heterojunction solar cells, *RSC Adv.*, 2014, **4**, 33279–33285.
70 S. Admassie, O. Inganäs, W. Mammo, E. Perzon and M. R. Andersson, Electrochemical and optical studies of the band gaps of alternating polyfluorene copolymers, *Synth. Met.*, 2006, **156**, 614–623.
71 T. Matsushima, G. H. Jin and H. Murata, Marked improvement in electroluminescence characteristics of organic light-emitting diodes using an ultrathin hole-injection layer of molybdenum oxide, *J. Appl. Phys.*, 2008, **104**, 054501.
72 X. Li, F. Xie, S. Zhang, J. Hou and W. C. H. Choy, MoOx and V2Ox as hole and electron transport layers through

functionalized intercalation in normal and inverted organic optoelectronic devices, *Light: Sci. Appl.*, 2015, **4**, e273.

73 M. Nyman, O. J. Sandberg, W. Li, S. Zeiske, R. Kerremans, P. Meredith and A. Armin, Requirements for making thick junctions of organic solar cells based on nonfullerene acceptors, *Sol. RRL*, 2021, **5**, 2100018.

74 X. Feng, Z. Xu, Z. Hu, C. Qi, D. Luo, X. Zhao, Z. Mu, C. Redshaw, J. W. Y. Lam, D. Ma and B. Z. Tang, Pyrene-based blue emitters with aggregation-induced emission features for high-performance organic light-emitting diodes, *J. Mater. Chem. C*, 2019, **7**, 2283–2290.

75 T. Chawanpunyawat, P. Chasing, P. Nalaoh, P. Maitarad, T. Sudyodsuk and V. Promarak, Rational design of chrysene-based hybridized local and charge-transfer molecules as efficient non-doped deep-blue emitters for simple-structured electroluminescent devices, *Chem. – Asian J.*, 2021, **16**, 4145–4154.

76 T. H. Han, M. R. Choi, C. W. Jeon, Y. H. Kim, S. K. Kwon and T. W. Lee, Ultrahigh-efficiency solution-processed simplified small-molecule organic light-emitting diodes using universal host materials, *Sci. Adv.*, 2016, **2**, e1601428.

77 J. H. Jou, S. Kumar, M. Singh, Y. H. Chen, C. C. Chen and M. T. Lee, Carrier modulation layer-enhanced organic light-emitting diodes, *Molecules*, 2015, **20**, 13005–13030.

78 F. So and D. Kondakov, Degradation mechanisms in small-molecule and polymer organic light-emitting diodes, *Adv. Mater.*, 2010, **22**, 3762–3777.

79 H. Usta, D. Alimli, R. Ozdemir, S. Dabak, Y. Zorlu, F. Alkan, E. Tekin and A. Can, Highly efficient deep-blue electroluminescence based on a solution-processable A-π-D-π-A oligo(p-phenyleneethynylene) small molecule, *ACS Appl. Mater. Interfaces*, 2019, **11**, 44474–44486.

80 L. J. Rothberg and A. J. Lovinger, Status of and prospects for organic electroluminescence, *J. Mater. Res.*, 1996, **11**, 3174–3187.

81 X. He, L. Gao, H. Liu, F. Liu, D. Jiang, C. Du, C. Sun and P. Lu, Highly efficient red fluorescent OLEDs based on diphenylacridine-naphthothiadiazole derivatives with upper level intersystem crossing, *Chem. Eng. J.*, 2021, **404**, 127055.

82 Y. Yu, M. Cang, W. Cui, L. Xu, R. Wang, M. Sun, H. Zhou, W. Yang and S. Xue, Efficient red fluorescent OLEDs based on aggregation-induced emission combined with hybridized local and charge transfer state, *Dyes Pigm.*, 2021, **184**, 108770.

83 M. J. Frisch, G. W. Trucks, H. B. Schlegel, G. E. Scuseria, M. A. Robb, J. R. Cheeseman, G. Scalmani, V. Barone, G. A. Petersson, H. Nakatsuji, X. Li, M. Caricato, A. V. Marenich, J. Bloino, B. G. Janesko, R. Gomperts, B. Mennucci, H. P. Hratchian, J. V. Ortiz, A. F. Izmaylov, J. L. Sonnenberg, D. Williams-Young, F. Ding, F. Lipparini, F. Egidi, J. Goings, B. Peng, A. Petrone, T. Henderson, D. Ranasinghe, V. G. Zakrzewski, J. Gao, N. Rega, G. Zheng, W. Liang, M. Hada, M. Ehara, K. Toyota, R. Fukuda, J. Hasegawa, M. Ishida, T. Nakajima, Y. Honda, O. Kitao, H. Nakai, T. Vreven, K. Throssell, J. A. Montgomery, Jr., J. E. Peralta, F. Ogliaro, M. J. Bearpark, J. J. Heyd, E. N. Brothers, K. N. Kudin, V. N. Staroverov, T. A. Keith, R. Kobayashi, J. Normand, K. Raghavachari, A. P. Rendell, J. C. Burant, S. S. Iyengar, J. Tomasi, M. Cossi, J. M. Millam, M. Klene, C. Adamo, R. Cammi, J. W. Ochterski, R. L. Martin, K. Morokuma, O. Farkas, J. B. Foresman and D. J. Fox, *Gaussian 16, Revision C.01*, Gaussian, Inc., Wallingford, CT, 2016.

